Wireless Personal Communications **2:** 335–356, 1996.

Transmission Performance Analysis of Multi-Carrier Modulation in Frequency Selective Fast Rayleigh Fading Channel

SHINSUKE HARA, MASUTADA MOURI, MINORU OKADA and
NORIHIKO MORINAGA
Department of Communication Engineering, Faculty of Engineering, Osaka University, 2-1 Yamada-oka, Suita-shi, Osaka 565, Japan (Tel.: 6-879-7738; Fax: 6-876-1923; E-mail: hara@comm.eng.osaka-u.ac.jp)

Abstract. In this paper, we discuss the transmission performance of Multi-Carrier Modulation (MCM) in frequency-selective fast Rayleigh fading channels. First, we optimize the transmission parameters of MCM with M-ary differential phase shift keying/differential detection (DPSK): *the guard duration* and *the number of sub-carriers* for frequency-selective fast Rayleigh fading channels, and then show the bit error rate (BER) performance of the optimized M-ary DPSK MCM. Next, we propose an MCM with pilot-assisted M-ary quadrature amplitude modulation/coherent detection (QAM), and discuss the BER performance when we reduce the number of pilot signals from the view-point of frequency-time utilization efficiency. Finally, we propose a two-stage frequency offset compensation method.

Key words: Multi-carrier modulation, M-ary DPSK, M-ary QAM, frequency offset compensation.

1. Introduction

Multi-Carrier Modulation (MCM) technique based on the Discrete Fourier Transform (DFT) and the Inverse DFT (IDFT) [?], which is called Orthogonal Frequency Division Multiplexing (OFDM), has been widely studied in various application fields such as data transmission over telephone line [?], digital audio broadcasting [?], land mobile communications [?, ?], indoor radio communications [?] and so on.

In the MCM, the whole bandwidth is divided into a number of sub-bands. Therefore, it is more resistant to frequency-selective multipath fading than a single-carrier modulation (SCM) technique, since each sub-carrier can operate at low data rate against frequency-selective fading. The MCM is a pre-distortion or, in a sense, a deterministic equalization technique at the transmitter.

The MCM with M-ary differential phase shift keying/differential detection (DPSK) is simple and attractive, because it requires no complicated carrier recovery circuit at the receiver. However, in order to support a higher data rate in a limited bandwidth, it is necessary to employ a bandwidth efficient modulation scheme such as M-ary quadrature amplitude modulation (QAM) at each sub-carrier.

In the design of MCM, it is essential to choose two transmission parameters: *the guard duration* Δ and *the number of sub-carriers* N carefully according to a given channel frequency-selectivity and time-selectivity, because they significantly affect the bit error rate (BER) performance. Many reports have shown the BER performance of MCM in fading channels, discussed the performance enhancement by coded modulation, and compared the BER with that of SCM using an adaptive equalization technique [7–9]. However, in their works, Δ and N are chosen empirically or according to the hardware limitation, and no report has been dedicated to their optimization problem in a frequency-selective fast Rayleigh fading channel.

For the MCM with M-ary QAM, it is necessary to support coherent detection at the receiver. A pilot-assisted 16QAM MCM [10] and a 16QAM MCM with an auto-regressive estimation method [11] have been proposed to realize the coherent detection, where a known pilot signal insertion and a fading normalization using a short training sequence are employed at each sub-carrier, respectively. However, it could be possible to estimate the instantaneous fading frequency distortion and its time variation without inserting a pilot signal periodically or employing an adaptive equalization at each sub-carrier, because the fading frequency correlation is generally high among sub-carriers.

Also, when a frequency offset is introduced in the radio channel, the BER of MCM degrades drastically, since severe inter-sub-carrier interference occurs because of the overlapping power spectra between sub-carriers. This sensitivity to frequency offset is often pointed out as a major MCM disadvantage. Therefore, it is essential to develop a fast and accurate frequency offset compensation method.

In this paper, we discuss the transmission performance of MCM in frequency selective fast Rayleigh fading channels. First, we optimize the transmission parameters of the M-ary DPSK MCM: *the guard duration* and *the number of sub-carriers* for frequency-selective fast Rayleigh fading channels, and then show the BER performance of the optimized M-ary DPSK MCM. Next, we propose a pilot-assisted M-ary QAM MCM, and discuss the BER performance when we reduce the number of pilot signals from the view-point of frequency-time utilization efficiency. Finally, we propose a two-stage frequency offset compensation method.

2. Multi-Carrier Modulation Technique

Figures 1(a) and (b) show the block diagrams of an MCM transmitter and receiver with N sub-carriers, respectively.

In the transmitter, the transmitted signal $s(t)$ is expressed as

$$s(t) = \sum_{i=-\infty}^{\infty} \sum_{k=0}^{N-1} \Re[c_{ki} e^{j2\pi f_k (t-iT_s)}] f(t - iT_s). \tag{1}$$

In Eq. (1), $\Re[\cdot]$ is the real part of $\cdot$ ($\Im[\cdot]$ the imaginary part of $\cdot$), and f_k is the frequency of the k-th sub-carrier:

$$f_k = f_0 + \frac{k}{t_s}, \tag{2}$$

where f_0 is the lowest frequency. $f(t)$ is the pulse waveform of each symbol defined as

$$f(t) = \begin{cases} 1 & (-\Delta \le t \le t_s) \\ 0 & (t < -\Delta, t > t_s), \end{cases} \tag{3}$$

where Δ and t_s are the guard duration and the observation duration, respectively, $T_s = \Delta + t_s$ is the symbol duration, and c_{ki} is an output at the k-th sub-carrier in time $[iT_s - \Delta, iT_s + t_s]$.

The transmitted signal $s(t)$ is the sum of N M-ary DPSK or M-ary QAM signals, and the required bandwidth is given by

$$B = \frac{2}{T_s} + \frac{N-1}{t_s} \approx \frac{N+1}{T_s} = \frac{N+1}{N} R, \tag{4}$$

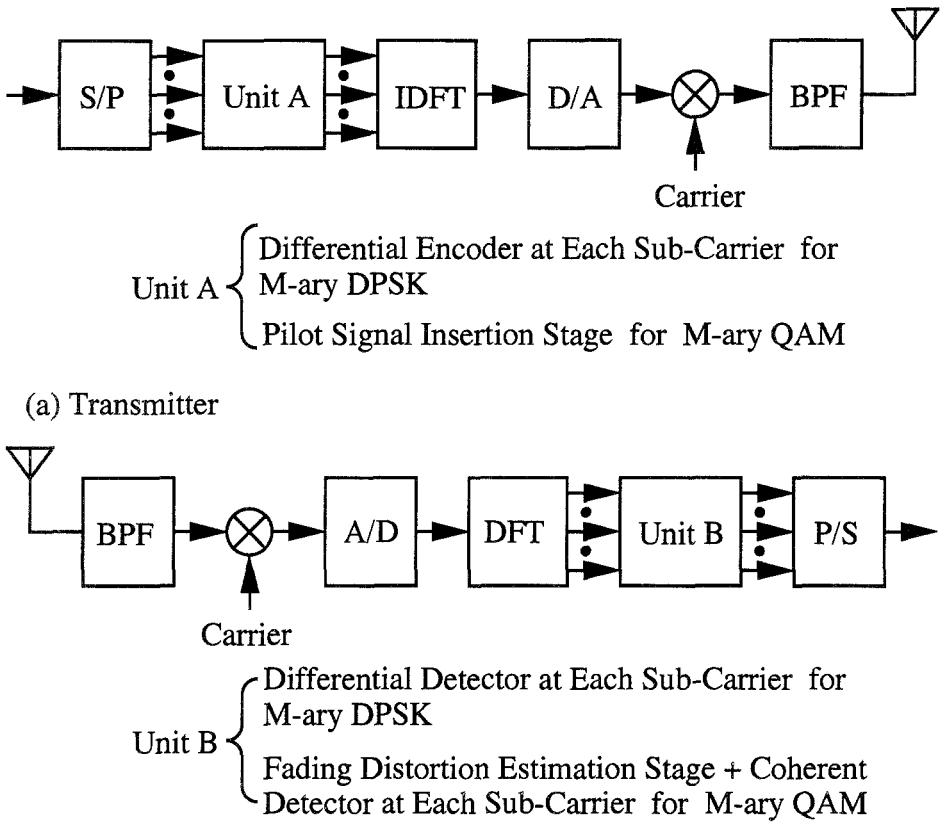

Figure 1. Block diagram of transmitter (a) and receiver (b) for MCM system.

where R (=N/T_s) is the total transmission rate (symbol/sec).

When M-ary DPSK signal is employed, the differential encoder and differential detector are used in the transmitter (Unit A) and receiver (Unit B), respectively, while when M-ary QAM signal is employed, the pilot signal insertion stage and coherent detector are used, as shown in Figures 1(a) and (b).

3. Frequency-Selective Fast Rayleigh Fading Channel

Through a radio channel, $s(t)$ is disturbed by multipath fading and the additive white Gaussian noise (AWGN). In the receiver, the received signal is expressed as

$$r(t) = \int_0^\infty s(t-\tau)h(\tau;t)d\tau + n(t), \tag{5}$$

where $h(\tau;t)$ is the impulse response of the channel at time t, and $n(t)$ is the complex AWGN.

Assuming that the radio channel is a *WSSUS* (wide sense stationary uncorrelated scattering) frequency-selective fast Rayleigh fading channel, it can be modeled as a tapped delay line where each tap gain is an independent complex Gaussian random variable. Therefore, $h(\tau;t)$ can be represented by

$$h(\tau;t) = \sum_{l=1}^{M_1+M_2} g_l(t)\delta(\tau-\tau_l), \tag{6}$$

$$0 \le \tau_l \le \Delta \quad (l = 1,\ldots,M_1),$$

$$\Delta < \tau_l < T_s \quad (l = M_1+1,\ldots,M_1+M_2), \tag{7}$$

where $\delta(t)$ is the Dirac delta function, $g_l(t)$ is the complex envelope of the signal received on the l-th path which is a complex Gaussian random variable with zero mean and variance σ_l^2, and τ_l is the propagation delay for the l-th path. The channel frequency-selectivity and channel time-selectivity are uniquely characterized by the multipath delay profile $\phi_c(\tau)$ (or the frequency autocorrelation function $\phi_C(\Delta f)$) and the Doppler power spectrum $S_c(\lambda)$ (or the time autocorrelation function $\phi_C(\Delta t)$).

4. Optimization of M-ary DPSK MCM

As the number of sub-carriers (N) increases, the transmission performance becomes more sensitive to the time selectivity because the wider symbol duration is less robust to the random FM noise. On the other hand, as N decreases, it becomes poor because the wider power spectrum of each sub-carrier is less robust to the frequency selectivity. Therefore, there exists an optimum value in N to minimize the BER.

Also, as the guard duration (Δ) increases, the transmission performance becomes poor because the signal transmission in the guard duration introduces the power loss. On the other hand, as Δ decreases, it becomes more sensitive to the frequency-selectivity because the shorter guard duration is less robust to the delay spread. Therefore, there exists an optimum value in Δ to minimize the BER.

For the M-ary DPSK MCM, we can easily optimize N and Δ, because the theoretical BER expression has been obtained in a closed form *for any multipath delay profile and any Doppler power spectrum* [15, 16] (see Appendix).

In order to show the BER performance in realistic frequency-selective fast Rayleigh fading channels, we assume:

- an exponential-type multipath delay profile with the root mean square (RMS) delay spread τ_{RMS} [12, 13] ($M_1 + M_2 = 20$),
- a Doppler power spectrum with the maximum Doppler frequency f_D when an omni-directional monopole antenna is used at the receiver [14] ($d = \pi f_D$).

Figures 2 and 3 show the optimum values of the number of sub-carriers (N) and guard duration (ΔR) versus the RMS delay spread ($\tau_{\mathrm{RMS}}R$) and the maximum Doppler frequency (f_D/R), respectively, where Δ, τ_{RMS} and f_D are normalized by the total transmission rate (R).

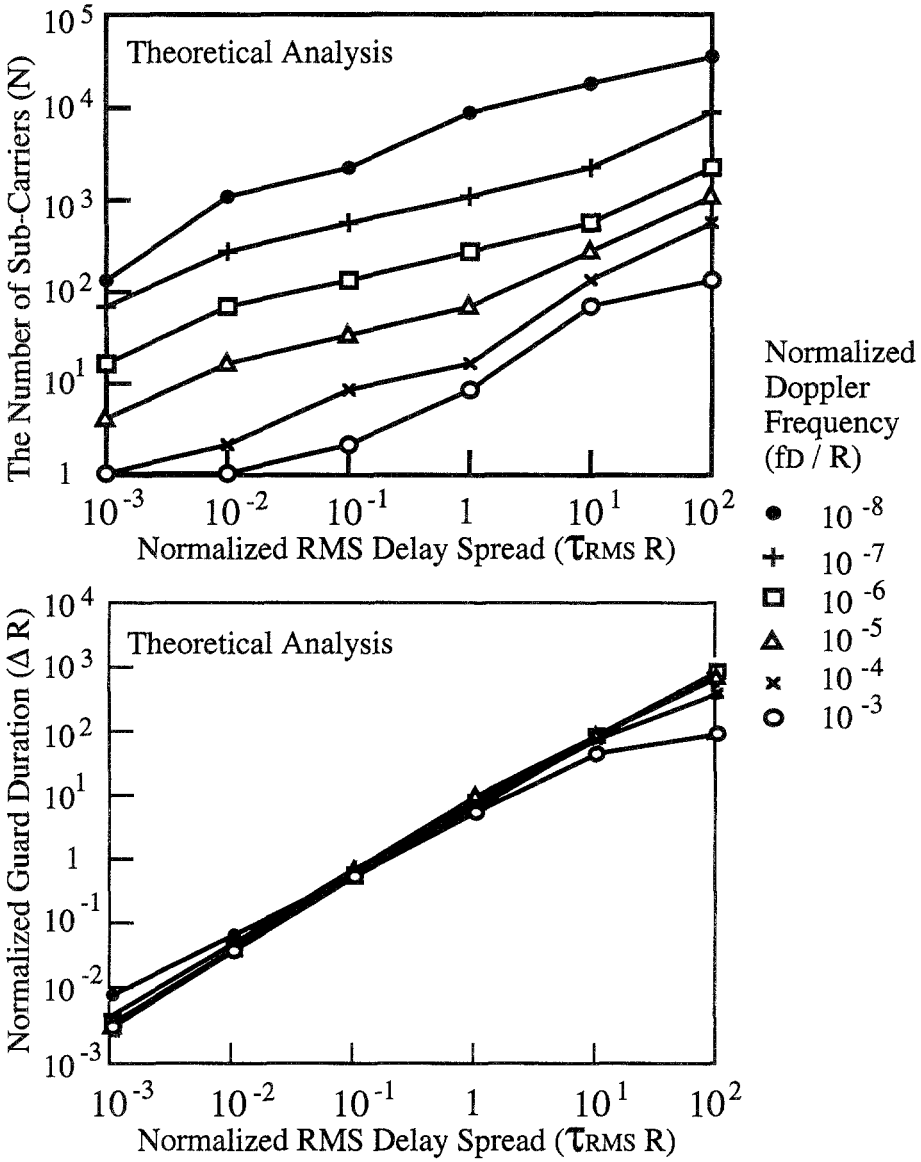

Figure 2. The number of sub-carriers (a) and guard duration (b) versus RMS delay spread.

Figure 4 shows the attainable BER of optimized quaternary DPSK MCM at the signal-to-noise energy ratio per bit (E_b/N_0) of 40 dB. When $[\tau_{\text{RMS}}R, f_D/R]$ introduced in the channel lies in the hatched region in this figure (roughly, $\tau_{\text{RMS}} \cdot f_D < 1.0 \times 10^{-6}$), the BER is less than $10^{-4.25} = 5.62 \times 10^{-5}$. Note that the BER of QDPSK SCM at E_b/N_0 of 40 dB in a frequency-non-selective slow Rayleigh fading channel (the BER lower bound) is $10^{-4.30} = 5.01 \times 10^{-5}$. Therefore, the BER degradation is less than 12.2%.

Figure 5 shows the BER of QDPSK MCM versus E_b/N_0 in a frequency-selective fast Rayleigh fading channel, where $N_{\text{opt}} = 128$ and $(\Delta/T_s)_{\text{opt}} = 0.06$ are optimized for $R =$ 8.192 Msymbol/sec, $f_D = 20$ Hz and $\tau_{\text{RMS}} = 100$ nsec (also, see Fig. 4). In this figure,

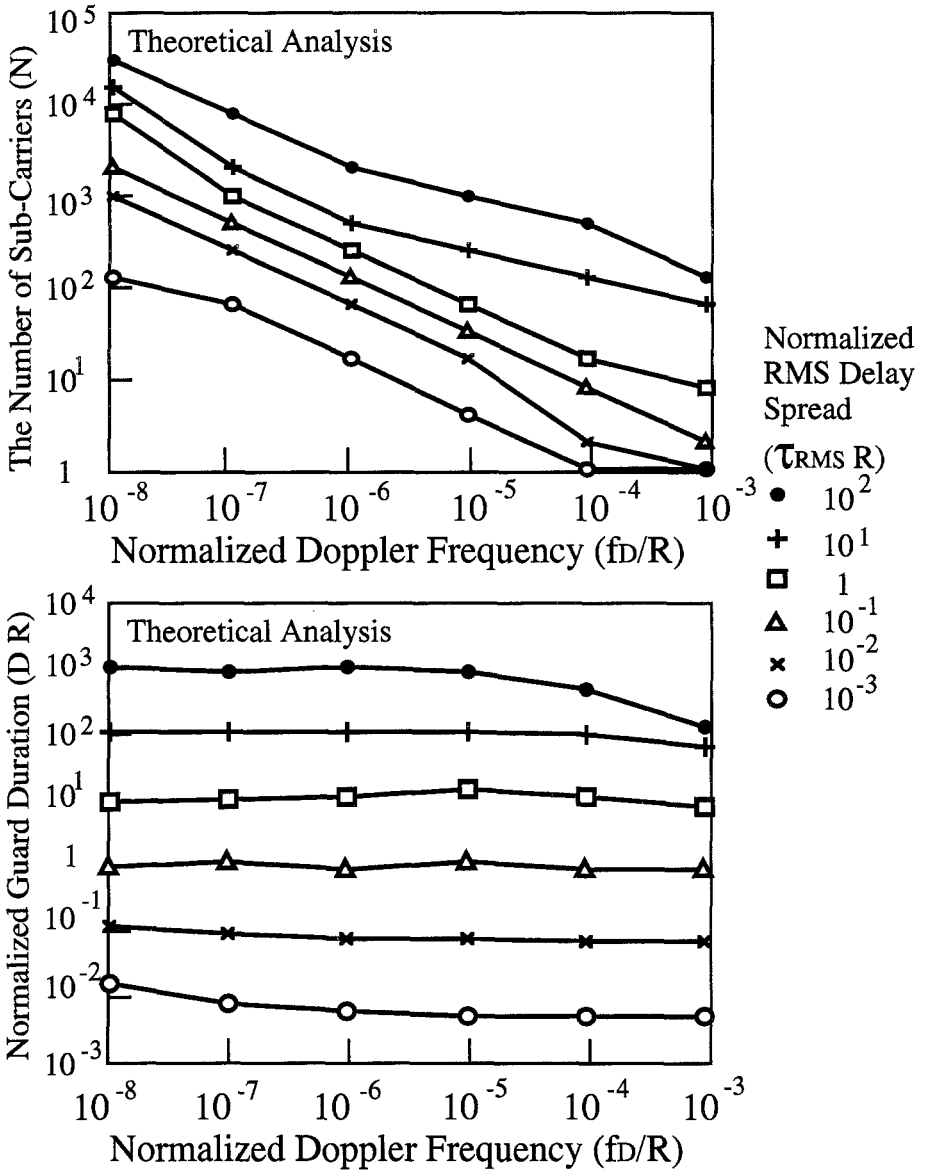

Figure 3. The number of sub-carriers (a) and guard duration (b) versus maximum Doppler frequency.

the BER of QDPSK SCM in a frequency-non-selective slow Rayleigh fading channel is also shown as the BER lower bound, which is given by Eq. (15) with

$$\rho = \frac{1}{1 + \frac{1}{\gamma}}, \tag{8}$$

where γ is the signal-to-noise power ratio.

The theoretical analysis and computer simulation results are in complete agreement, and there is little difference in the BER between the optimized MCM and the lower bound.

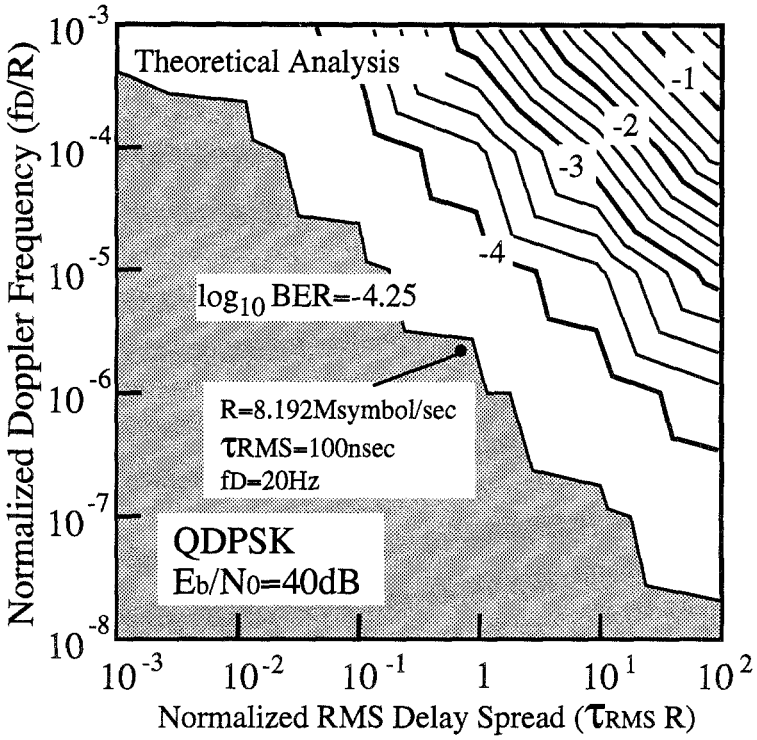

Figure 4. Attainable BER of optimized QDPSK MCM.

Figure 6 shows the BER of the optimized QDPSK MCM in a frequency-non-selective slow Rayleigh fading channel. There is also little difference in the BER between the optimized MCM and the lower bound. Therefore, in this case, the MCM optimized for the channel maximum Doppler frequency and maximum RMS delay spread can keep the minimum BER even when the channel time-selectively and frequency-selectivity change.

Figure 7 shows the BER of binary DPSK MCM and octonary DPSK MCM versus E_b/N_0 in a frequency-selective fast Rayleigh fading channel, where $N_{\text{opt}} = 128$ and $(\Delta/T_s)_{\text{opt}} = 0.06$ are also optimized for $R = 8.192$ Msymbol/sec, $f_D = 20$ Hz and $\tau_{\text{RMS}} = 100$ nsec. For BDPSK and ODPSK, there is also little difference in the BER between the optimized MCM and the lower bound.

5. Pilot-Assisted M-ary QAM MCM

For the M-ary QAM MCM, we cannot easily determine N_{opt} and $\Delta_{\text{opt}}R$, because we have not obtained the theoretical BER expression yet. Therefore, we have to resort to computer simulation to analyze the BER.

However, for a given τ_{RMS}, f_D and R, N_{opt} and $\Delta_{\text{opt}}R$ could depend not on the modulation/demodulation scheme employed at each sub-carrier but on the relation among them. Therefore, in this section, we use the optimum N and Δ derived in the previous section.

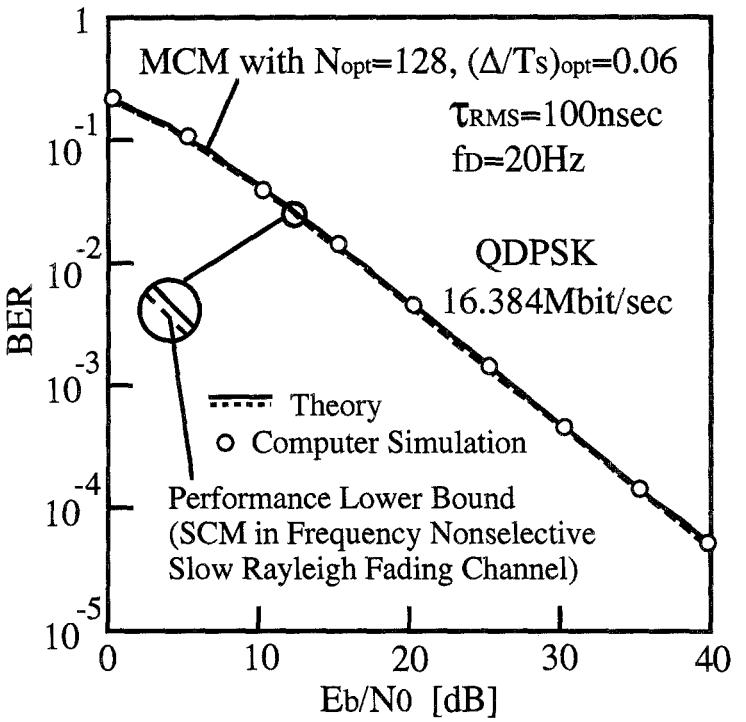

Figure 5. BER of QDPSK MCM in frequency-selective fast Rayleigh fading channel.

5.1. Two Dimensional (Frequency-Time) Pilot Signal Insertion

In the transmitter, the pilot signal insertion stage inserts a known pilot signal having a maximum amplitude in every N_T sub-carriers and N_f symbols (see Fig. 8).

In the receiver, for sub-carriers having no pilot signals, the reference signals are recovered by interpolation (partially, extrapolation) of pilot signals in the frequency domain (see Fig. 9). After the reference signal recovery, the coherent detection at each sub-carrier is done by interpolation of pilot signals (or reference signals) in the time domain.

5.2. Reference Signal Recovery in Frequency Domain

When $N = k \cdot N_f + 1$ (k: integer), all the reference signals can be recovered only by interpolation, because sub-carriers at both the lowest frequency and the highest frequency can be chosen as the pilot-inserted channel. However, when $N \neq k \cdot N_f + 1$, extrapolation is partially needed. In this case, if the lowest sub-carrier is always chosen as the pilot-inserted channel, then the reference signal in the highest sub-carrier is recovered by extrapolation, and it degrades the BER. To avoid the BER degradation, the lowest and highest sub-carriers are alternately chosen as the pilot-inserted channel.

Figure 10 shows the error variance of the recovered reference signal versus the RMS delay spread. The performance of the polynomial interpolation is worse because of the wild oscillation between the tabulated points. As the delay spread increases, the error variance increases. For the cubic spline interpolation, the performance of $N_f = 8$ is almost identical to that of $N_f = 4$.

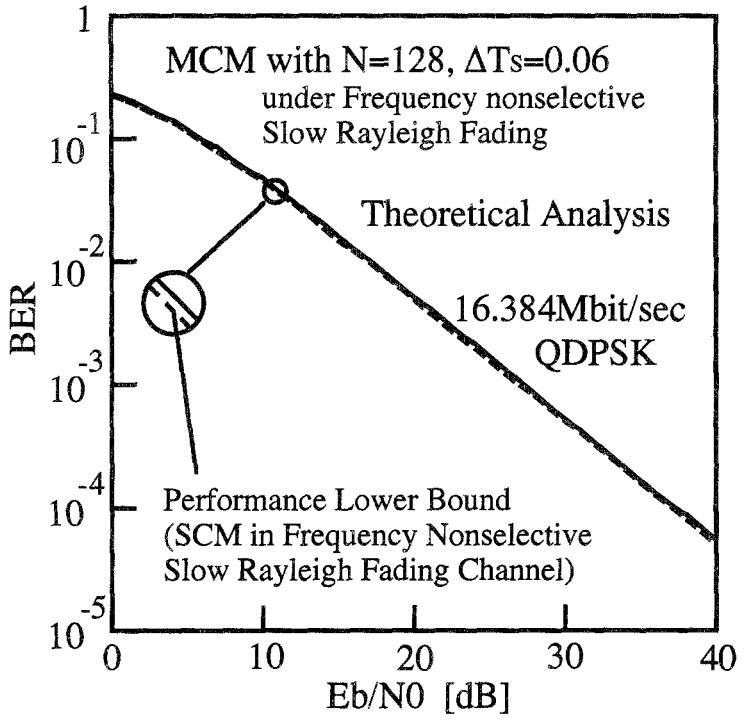

Figure 6. BER of QDPSK MCM in frequency-non-selective slow Rayleigh fading channel.

5.3. Coherent Detection (Reference Signal Recovery in Time Domain)

At each sub-carrier, the pilot signals or reference signals are interpolated between $t = l \cdot N_T$ and $t = (l+1) \cdot N_T$ (l: integer), and finally the coherent detection is carried out.

The Pilot-Assisted M-ary QAM MCM satisfying $N = k \cdot N_f + 1$ sometimes shows interesting phenomena in the BER performance.

Figures 11 and 12 show the BER performance of 16QAM MCM versus the RMS delay spread, where $N = 64$ and $\Delta/T_s = 0.015$ are optimized for $R = 2.048$ Msymbol/sec, $\tau_{\text{RMS}} = 50$ nsec and $f_D = 20$ Hz. Figure 11 uses the linear interpolation in both frequency and time domains, and Fig. 12 the cubic spline interpolation in the frequency domain and the linear interpolation in the time domain.

The BER of $N_f = 3$ is superior to that of $N_f = 1$ in Fig. 11, and the BERs of $N_f = 3$ and $N_f = 7$ to that of $N_f = 1$ in Fig. 12. It is because as N_f increases, the accuracy of reference signal recovery is reduced whereas the effect of noise is suppressed by the interpolation. Also, in both figures, there is little difference in the BER performance between $N_T = 2$ and $N_T = 50$.

Figure 13 shows the BER performance of 16QAM MCM, 64QAM MCM and 256QAM MCM versus E_b/N_0 in a frequency-selective fast Rayleigh fading channel, where $N_{\text{opt}} = 128$ and $(\Delta/T_s)_{\text{opt}} = 0.06$ are optimized for $R = 8.192$ Msymbol/sec, $\tau_{\text{RMS}} = 100$ nsec and $f_D = 20$ Hz. In this figure, the BER of SCM in a frequency-non-selective slow Rayleigh

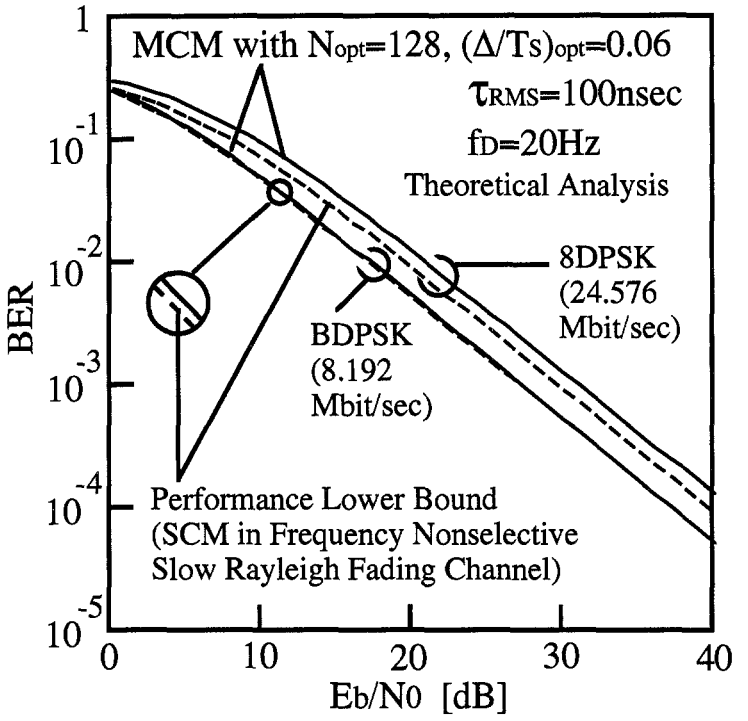

Figure 7. BER of BDPSK MCM and 8DPSK MCM in frequency-selective fast Rayleigh fading channel.

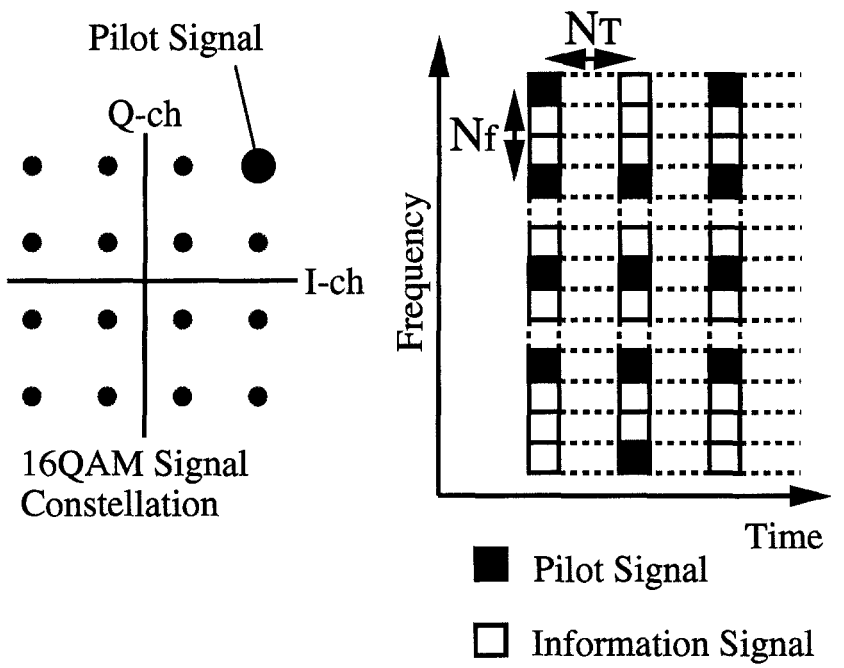

Figure 8. Pilot signal insertion.

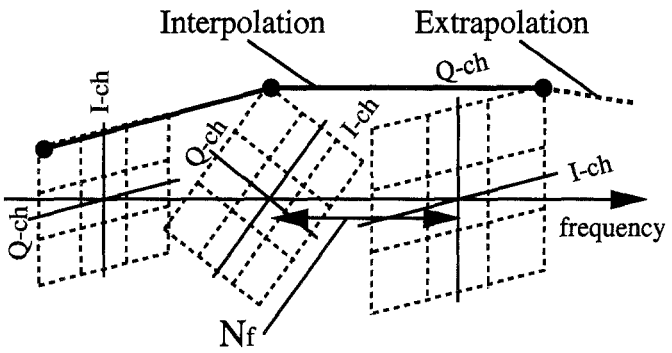

Figure 9. Interpolation (and extrapolation) in frequency domain.

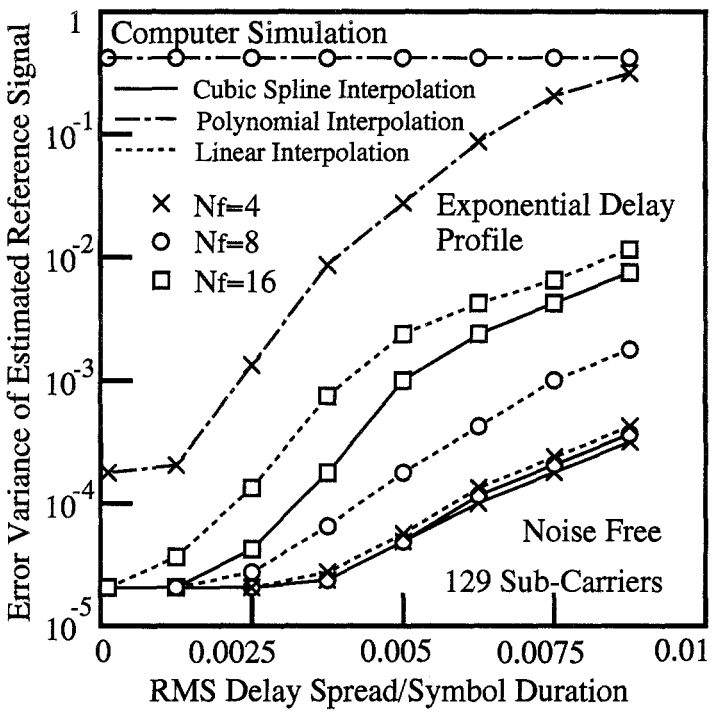

Figure 10. Error variance versus RMS delay spread.

fading channel is given by [17]

$$\text{BER(16QAM)} = \frac{3}{8}\left[1 - \sqrt{\frac{\gamma}{10+\gamma}}\right], \tag{9}$$

$$\text{BER(64QAM)} = \frac{7}{24}\left[1 - \sqrt{\frac{\gamma}{42+\gamma}}\right], \tag{10}$$

$$\text{BER(256QAM)} = \frac{15}{64}\left[1 - \sqrt{\frac{\gamma}{170+\gamma}}\right]. \tag{11}$$

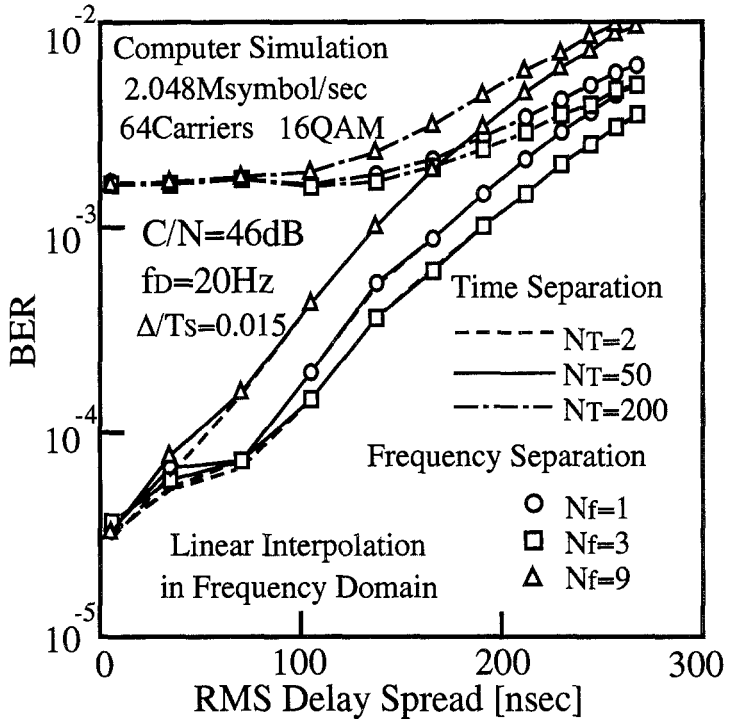

Figure 11. BER versus RMS delay spread (linear interpolation).

The BER of the optimized M-ary QAM MCM in the frequency-selective fast Rayleigh fading channel is almost the same as that of the M-ary QAM SCM in the frequency-non-selective slow Rayleigh fading channel.

6. Frequency Offset Compensation Method

We have assumed a perfect DFT window timing synchronization and a perfect carrier frequency synchronization in the previous sections. In this section, we consider the problem of carrier frequency synchronization.

Figure 14 shows the BER of the optimized QDPSK MCM versus the frequency offset normalized by the sub-carrier separation ($f_{\text{off}} \cdot t_s$) in a frequency-selective fast Rayleigh fading channel with $f_D = 20$ Hz and $\tau_{\text{RMS}} = 100$ nsec [19]. The BER degrades rapidly as the frequency offset increases, because the spectrally overlapping characteristic of sub-carriers results in severe inter-sub-carrier interference. In this paper, we propose a two-stage frequency compensation method [18].

Figure 15 shows the time-frequency format of a signal burst. The header is composed of two parts, a preamble for the DFT window timing synchronization and a group of pilot signals for the carrier frequency synchronization, where the same pseudo-random binary sequence (PRBS) is inserted at $t = 1 \cdot T_s$ and $t = 2 \cdot T_s$ and a differentially encoded PRBS at $t = 3 \cdot T_s$.

The frequency offset is generally expressed as

$$f_{\text{off}} = N_{\text{off}} \cdot (1/t_s) + f'_{\text{off}}, \tag{12}$$

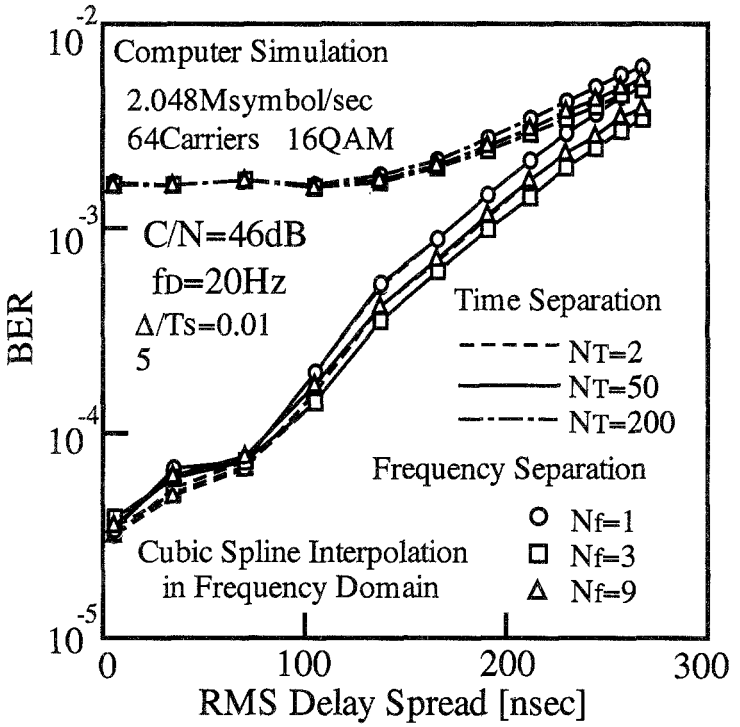

Figure 12. BER versus RMS delay spread (cubic spline interpolation).

where N_{off} is an integer and $|f'_{\text{off}} \cdot t_s| \leq 0.5$. The first and second stages estimate f'_{off} and N_{off}, respectively.

6.1. Frequency Offset Compensation Stage 1

Assume that the preamble has introduced the perfect DFT window timing synchronization. Observing the phase shift between the DFT outputs at $t = 1 \cdot T_s$ and $t = 2 \cdot T_s$ of the m-th sub-carrier ($\Delta\theta^m$), we can estimate f'^m_{off} as:

$$\widehat{f'^m_{\text{off}}} = \frac{1}{2\pi T_s}\Delta\theta^m = \frac{1}{2\pi T_s}\tan^{-1}\frac{\Im[r_{m,2}r^*_{m,1}]}{\Re[r_{m,2}r^*_{m,1}]}, \tag{13}$$

where $r_{m,i}$ is the DFT output of the m-th sub-carrier at $t = i \cdot T_s$ $(i = 1, 2)$. Then, averaging $\Delta\theta^m$ $(m = 0, \ldots, N-1)$ over all the sub-carriers yields

$$\widehat{f'_{\text{off}}} = \frac{1}{2\pi N T_s}\sum_{m=0}^{N-1}\tan^{-1}\frac{\Im[r_{m,2}r^*_{m,1}]}{\Re[r_{m,2}r^*_{m,1}]}. \tag{14}$$

Figure 14 shows the BER for the frequency offset compensation 1 using a PRBS with a period of 128, where 0 is added to the 7-stage M-sequence (the PRBS is used to reduce

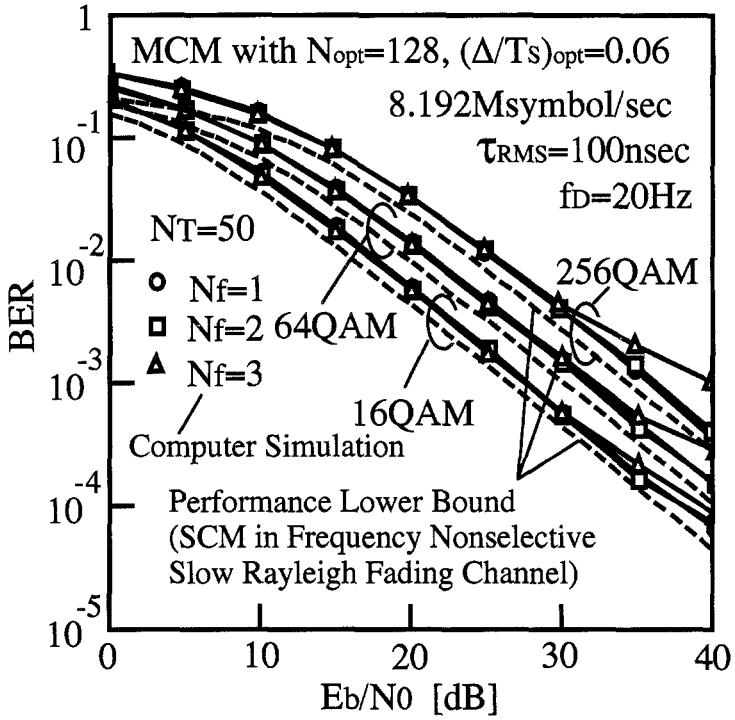

Figure 13. BER of 16QAM MCM, 64QAM MCM and 256QAM MCM in frequency-selective fast Rayleigh fading channel.

the envelop peak value). The first stage can remove the frequency offset accurately for $|f'_{\text{off}} \cdot t_s| \leq 0.5$, and make the BER almost the same as the lower bound.

Figure 16 shows the RMS frequency error normalized by the sub-carrier separation versus the RMS delay spread. As the delay spread becomes large, the frequency error slightly improves, because the frequency correlations among sub-carriers become low.

The performance of stage 1 depends on the number of sub-carriers, because the effect of noise can be reduced by the averaging process given by Eq. (14). Figure 17 shows the BER versus the number of sub-carriers, where a PRBS with a period of K is used for the case of K sub-carriers. Using 8 or 16 sub-carriers, the stage 1 can sufficiently suppress the effect of noise. This compensation method 1 is principally identical to Moose's method [20].

6.2. Frequency Offset Compensation Stage 2

Using the autocorrelation characteristic of the differentially detected PRBS at $t = 3 \cdot T_s$ (if there are few errors in the PRBS), we can remove the frequency ambiguity N_{off} (see Fig. 18).

Fig. 19 shows the BER for the frequency offset compensation 1+2. The BER becomes worse for $6 < |f_{\text{off}} \cdot t_s| < 10$, because the frequency offset and the guard duration causes a wrong phase shift in the differential detection process ($N_{\text{off}} \cdot \Delta/T_s \approx 0.5$), and it results in a lot of errors in the PRBS. Consequently, the two-stage method can estimate the frequency offset accurately for $|f_{\text{off}} \cdot t_s| \leq 6$. However, if we set the guard duration in the header to be zero, we can make the frequency acquisition range wider.

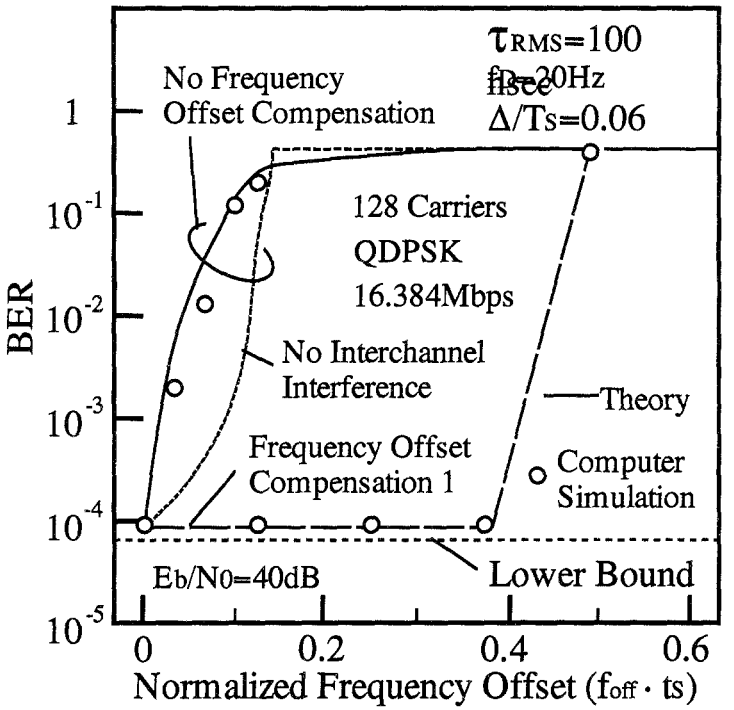

Figure 14. BER of QDPSK MCM versus frequency offset in frequency-selective fast Rayleigh fading channel.

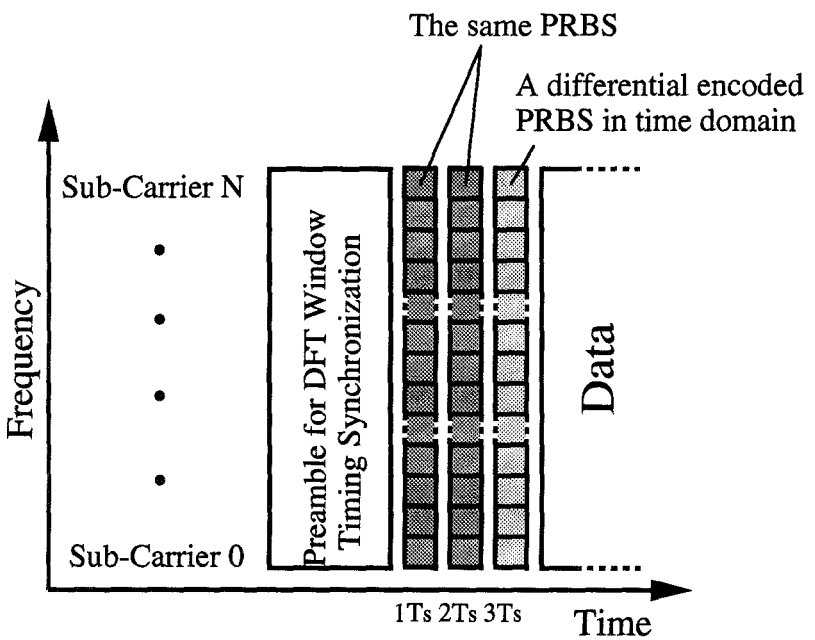

Figure 15. Signal burst format for frequency offset compansation.

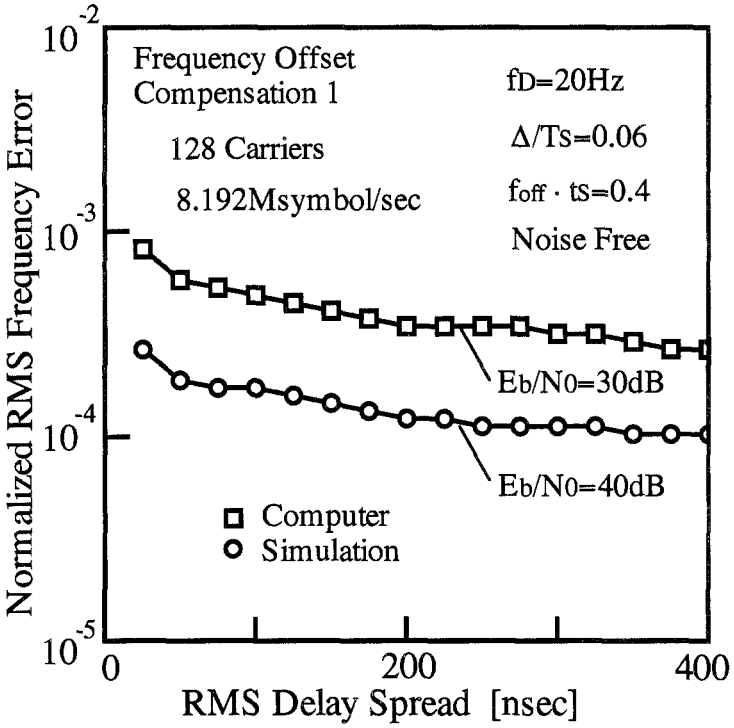

Figure 16. RMS frequency error versus RMS delay spread.

7. Conclusions

We have discussed the transmission performance of Multi-Carrier Modulation in frequency-selective fast Rayleigh fading channels.

We have shown the design method of *the guard duration* (Δ) and *the number of sub-carriers* (N) of MCM for a given frequency-selective fast Rayleigh fading channel with f_D and τ_{RMS} and a given total transmission rate (R), and have demonstrated the region of f_D and τ_{RMS} where Multi-Carrier Modulation can be an effective method against frequency-selectivity and time-selectivity introduced by the channel.

Then, we have designed the optimized M-ary DPSK MCM for $f_D = 20$ Hz, $\tau_{\mathrm{RMS}} = 100$ nsec and $R = 8.192$ Msymbol/sec, and have shown the BER performance is almost the same as the lower bound, the BER of the M-ary DPSK single carrier modulation in a frequency-non-selective slow Rayleigh fading channel.

Next, we have proposed a pilot-assisted QAM MCM, and have shown the BER performance of 16QAM MCM, 64QAM MCM and 256QAM MCM when we reduce the number of pilot signals from the view-point of frequency-time utilization efficiency.

Finally, we have proposed a two-stage frequency offset compensation method. For the optimized QDPSK MCM with $R = 8.192$ Msymbol/sec, $N_{\mathrm{opt}} = 128$ and $(\Delta/T_s)_{\mathrm{opt}} = 0.06$, the two-stage method can accurately estimate the frequency offset for $|f_{\mathrm{off}}| \leq 408.5$ kHz in the frequency-selective fast Rayleigh fading channel with $f_D = 20$ Hz and $\tau_{\mathrm{RMS}} = 100$ nsec.

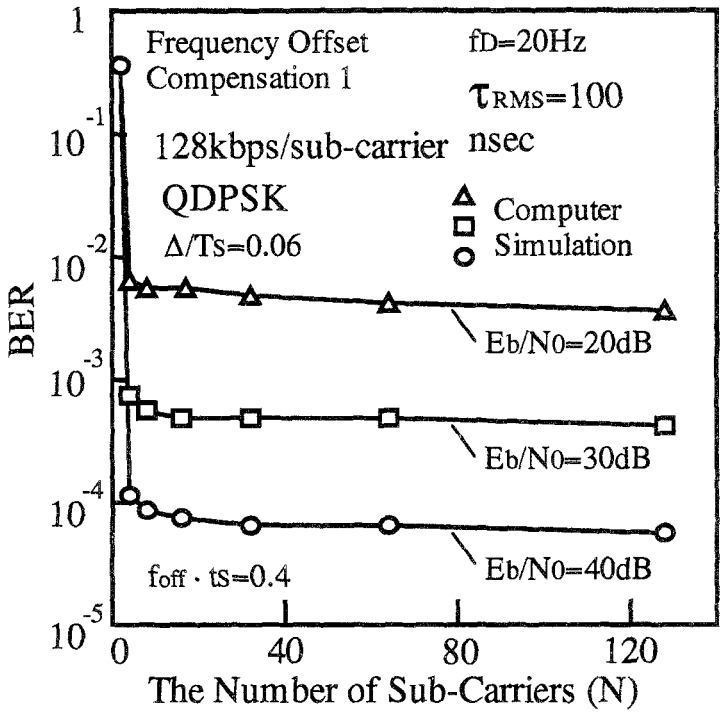

Figure 17. BER versus the number of sub-carriers.

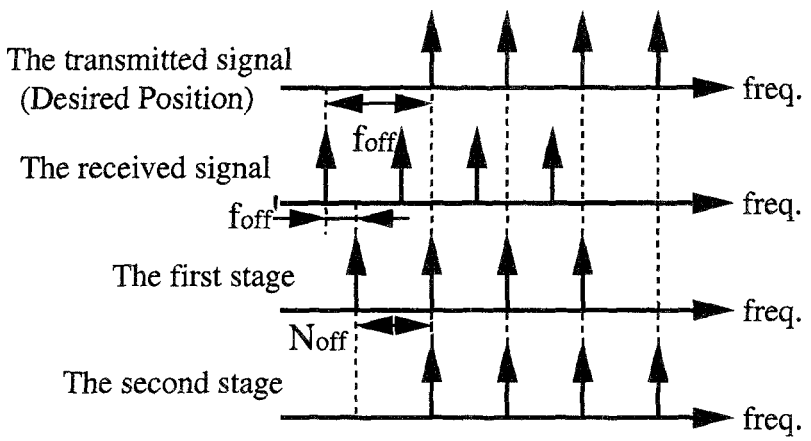

Figure 18. Frequency offset compensation.

Appendix

The BER is given by

$$\mathrm{BER} = \frac{\sqrt{1-\rho^2\cos^2\left(\frac{\pi}{M}\right)} - \rho\sin\left(\frac{\pi}{M}\right)}{2\sqrt{1-\rho^2\cos^2\left(\frac{\pi}{M}\right)}}. \tag{15}$$

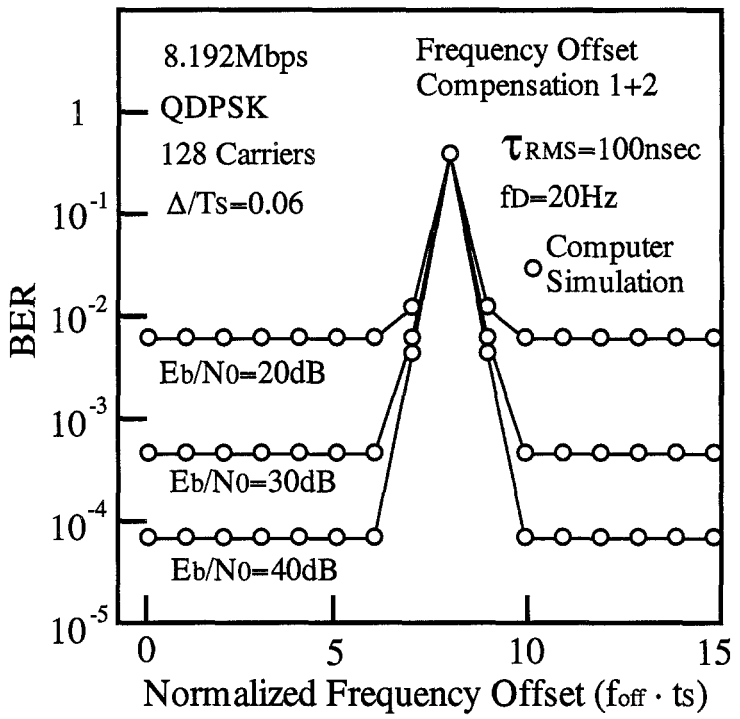

Figure 19. BER of QDPSK MCM versus frequency offset in frequency–selective fast Rayleigh fading channel.

In the above equation, ρ is the normalized correlation between the outputs (Fourier coefficients) of the m-th sub-carrier ($m = 0, \ldots, N-1$) at iT_s and $(i-1)T_s$ approximately given by

$$\rho = \frac{\sigma_{S1}^2}{\sigma_{S2}^2 + \sigma_I^2 + \sigma_n^2}, \tag{16}$$

where σ_n^2 is the noise power, and σ_{S1}^2, σ_{S2}^2 and σ_I^2 are given by

$$\begin{aligned}\sigma_{S1}^2 &= \sum_{l=1}^{M_1} \sigma_l^2 \left\{1 - \left(\frac{d}{R}\right)^2 \left(\frac{(N-\Delta R)^2}{6} + N^2\right)\right\} \\ &\quad + \sum_{l=M_1+1}^{M_1+M_2} \sigma_l^2 \frac{(N-\tau_l R)^2}{(N-\Delta R)^2} \cdot \left\{1 - \left(\frac{d}{R}\right)^2 \left(\frac{(N-\tau_l R)^2}{6} + N^2\right)\right\},\end{aligned} \tag{17}$$

$$\begin{aligned}\sigma_{S2}^2 &= \sum_{l=1}^{M_1} \sigma_l^2 \left\{1 - \left(\frac{d}{R}\right)^2 \frac{(N-\Delta R)^2}{6}\right\} \\ &\quad + \sum_{l=M_1+1}^{M_1+M_2} \sigma_l^2 \frac{(N-\tau_l R)^2}{(N-\Delta R)^2} \cdot \left\{1 - \left(\frac{d}{R}\right)^2 \frac{(N-\tau_l R)^2}{6}\right\}\end{aligned}$$

$$+\sum_{l=M_1+1}^{M_1+M_2}\sigma_l^2\frac{(-\Delta R+\tau_l R)^2}{(N-\Delta R)^2}\cdot\left\{1-\left(\frac{d}{R}\right)^2\frac{(-\Delta R+\tau_l R)^2}{6}\right\}, \tag{18}$$

and

$$\begin{aligned}\sigma_I^2 = &\sum_{l=1}^{M_1}\sum_{\substack{k=0\\k\neq m}}^{N-1}\sigma_l^2\frac{\left(\frac{d}{R}\right)^2(N-\Delta R)^2}{2\pi^2(k-m)^2}\\
&+\sum_{l=M_1+1}^{M_1+M_2}\sum_{\substack{k=0\\k\neq m}}^{N-1}\sigma_l^2\left\{\frac{\left(\frac{d}{R}\right)^2(N-\tau_l R)^2}{2\pi^2(k-m)^2}\cdot\cos\left(\frac{2\pi(k-m)(N-\tau_l R)}{N-\Delta R}\right)\right.\\
&+\frac{\left(\frac{d}{R}\right)^2(N-\Delta R)(N-\tau_l R)}{\pi^3(k-m)^3}\cdot\sin\left(\frac{2\pi(k-m)(N-\tau_l R)}{N-\Delta R}\right)\\
&+\left(\frac{1}{2\pi^2(k-m)^2}+\frac{3\left(\frac{d}{R}\right)^2(N-\Delta R)^2}{4\pi^4(k-m)^4}\right)\\
&\cdot\left(1-\cos\left(\frac{2\pi(k-m)(N-\tau_l R)}{N-\Delta R}\right)\right)\\
&+\frac{\left(\frac{d}{R}\right)^2(-\Delta R+\tau_l R)^2}{2\pi^2(k-m)^2}\cos\left(\frac{2\pi(k-m)(-\Delta R+\tau_l R)}{N-\Delta R}\right)\\
&+\frac{\left(\frac{d}{R}\right)^2(N-\Delta R)(-\Delta R+\tau_l R)}{\pi^3(k-m)^3}\sin\left(\frac{2\pi(k-m)(-\Delta R+\tau_l R)}{N-\Delta R}\right)\\
&+\left(\frac{1}{2\pi^2(k-m)^2}+\frac{3\left(\frac{d}{R}\right)^2(N-\Delta R)^2}{4\pi^4(k-m)^4}\right)\\
&\left.\cdot\left(1-\cos\left(\frac{2\pi(k-m)(-\Delta R+\tau_l R)}{N-\Delta R}\right)\right)\right\},\end{aligned} \tag{19}$$

where d is a coefficient when the time autocorrelation function is approximated as

$$\phi_C(\Delta t)\approx 1-(d\Delta t)^2. \tag{20}$$

For example, when we use an omni-directional monopole antenna at the receiver [14], d is written as

$$d=\pi f_D, \tag{21}$$

where f_D is the maximum Doppler frequency.

For $\rho\approx 1.0$, Eq. (15) becomes

$$\text{BER}=\frac{1}{2}(1-\rho). \tag{22}$$

Therefore, we can use Eq. (22) to evaluate the BER for any M-ary DPSK MCM, and the minimization problem of the BER results in the maximization problem of ρ for N and Δ.

Acknowledgement

The authors wish to thank Mqhele Enock–Hershal Dlodlo for his helpful comments, which have led to improvements of the paper.

References

1. S.B. Weinstein and P.M. Ebert: "Data Transmission By Frequency-Division Multiplexing Using the Discrete Fourier Transform," IEEE Trans. on Commun. Tech., Vol. COM-19, No. 5, pp. 628–634, 1971.
2. J.A.C. Bingham: "Multicarrier Modulation for Data Transmission: An Idea Whose Time Has Come," IEEE Commun. Magazine, 28, No. 5, pp. 5–14, 1990.
3. B.L. Floch, R. Halbert-Lassalle and D. Castelain: "Digital Sound Broadcasting to Mobile Receivers," IEEE Trans. on Consumer Electronics, 35, No. 3, pp. 493–503, 1989.
4. L.J. Cimini: "Analysis and Simulation of a Digital Mobile Channel Using Orthogonal Frequency Division Multiplexing," IEEE Trans. on Commun., Vol. COM-33, No. 6, pp. 665–675, 1985.
5. K. Fazel and L. Papke: "On the Performance of Convolutionally-Coded CDMA/OFDM for Mobile Communication System," Proceedings of the Fourth International Symposium on Personal, Indoor and Mobile Radio Communications (PIMRC'93), pp. 468–472, Yokohama, Japan, 8–11 September, 1993.
6. N. Yee, J.-P. Linnartz and G. Fettweis: "Multi-Carrier CDMA in Indoor Wireless Radio Networks," Proceedings of The Fourth International Symposium on Personal, Indoor and Mobile Radio Communications (PIMRC'93), pp. 109–113, Yokohama, Japan, 8–11 September, 1993.
7. H. Xue, A. Nix, M. Beach and J. McGeehan: "Air Interface Considerations for Wireless LANs," Proceedings of The Fourth European Conference on Radio Relay Systems (ECRR'93), pp. 45–50, Edinburgh, UK, 11–14 October, 1993.
8. H. Sari and I. Jeanclaude: "An Analysis of Orthogonal Frequency-Division Multiplexing for Mobile Radio Applications," Proceedings of 1994 IEEE 44th Vehicular Technology Conference, pp. 1635–1639, Stockholm, Sweden, 8–10 June, 1994.
9. M. Aldinger: "Multicarrier COFDM Scheme in High Bitrate Radio Local Area Networks," Proceedings of ICCC Regional Meeting on Wireless Computer Networks (WCN), pp. 969–973, The Hague, The Netherlands, 21–23 September, 1994.
10. M. Saito, S. Moriyama and O. Yamada: "A Digital Modulation Method for Terrestrial Digital TV Broadcasting Using Trellis Coded OFDM and its Performance," Proceedings of IEEE Global Telecommunications Conference (GLOBECOM) '92, pp. 1694–1698, Orlando, Florida, USA, 6–9 December, 1992.
11. S.K. Wilson, R.E. Khayata and J.M. Cioffi: "16QAM Modulation with Orthogonal Frequency Division Multiplexing in a Rayleigh-Fading Environment," Proceedings of 1994 IEEE 44th Vehicular Technology Conference, pp. 1660–1664, Stockholm, Sweden, 8–10 June, 1994.
12. A.D.M. Saleh and R.A. Valenzuela: "A statistical Model for Indoor Multipath Propagation," *IEEE Journal on Selected Areas in Commun.*, Vol. SAC-5, No. 2, pp. 128–137, 1987.
13. E. Moriyama, M. Mizuno, Y. Nagata, Y. Furuya, I. Kamiya and S. Hattori: "Indoor Radio Propagation Study by Multipath Characteristics Measurement," IEICE technical report (in Japanese), RCS90-57, pp. 17–24.
14. W.C. Lee: "Mobile Communications Engineering," McGraw-Hill, 1982.
15. S. Hara, K. Fukui and N. Morinaga: "Multicarrier Modulation Technique for Broadband Indoor Wireless Communications," Proceedings of The Fourth International Symposium on Personal, Indoor and Mobile Radio Communications (PIMRC'93), pp. 132–136, Yokohama, Japan, 8–11 September, 1993.
16. S. Hara, M. Okada and N. Morinaga: "Multicarrier Modulation Technique for Wireless Local Area Networks," Proceedings of The Fourth European Conference on Radio Relay Systems (ECRR'93), pp. 33–38, Edinburgh, UK, 11–14 October, 1993.
17. M. Kuwahara: "Digital Microwave Communications (in Japanese)," Kikaku Center, 1984.
18. S. Hara and N. Morinaga: "System Performances of Multicarrier Modulation in Fading Channels (in Japanese)," ITE Technical Report, Vol.18, No.11, pp. 39–44, Feb., 1994.
19. K. Fukui: "Frequency Offset Compensation Technique for Multi-Carrier Modulation (in Japanese)," Master's Thesis, Osaka University, Osaka, Japan, Mar., 1994.
20. P.H. Moose: "A Technique for Orthogonal Frequency Division Multiplexing Frequency Offset Correction," IEEE Trans. on Commun., Vol. COM-42, No. 10, pp. 2908–2914, 1994.

Shinsuke Hara was born in Osaka, Japan, on January 22, 1962. He received the B.Eng., M.Eng. and Ph.D. degrees in communication engineering from Osaka University in 1985, 1987 and 1990, respectively. Since 1990 he has been with the Department of Communication Engineering at Osaka University, where he is now an Assistant Professor. His research interests include satellite, mobile and indoor wireless communication systems, and digital signal processings. Dr. Hara is also a member of the IEICE of Japan.

Masutada Mouri was born in Hyougo, Japan, on July 16, 1971. He received the B.Eng. degree in communication engineering from Osaka University in 1994. He is currently pursuing for the M.Eng. degree at the Department of Communication Engineering, Osaka University. His research interests are in the areas of mobile and indoor wireless communication systems.

Minoru Okada was born in Tokushima, Japan, on March 4, 1958. He received the B.Eng. degree in communication engineering from University of Electro-Communications, Tokyo, Japan, in 1990, and the M.Eng. degree from Osaka University, Osaka, Japan, in 1992. Since 1993, he has been with the Department of Electrical Engineering at Osaka University, where he is now an Assistant Professor. His research interests are in the areas of mobile and indoor wireless communication systems. Dr. Osaka is also a member of the IEICE of Japan.

Norihiko Morinaga received the B.Eng. degree in electrical engineering from Shizuoka University, Shizuoka, Japan, in 1963, and the M.Eng. and Ph.D. degrees from Osaka University, Osaka, Japan, in 1965 and 1968, respectively. He is currently a Professor in the Department of Communication Engineering at Osaka University, working in the areas of radio, mobile, satellite, and optical communication systems, and EMC. Dr. Morinaga is also a member of the IEICE and ITE of Japan.